PCCP

PAPER

View Article Online
View Journal | View Issue

Check for updates

Cite this: *Phys. Chem. Chem. Phys.*, 2024, **26**, 10832

Photoswitching of arylazopyrazoles upon S_1 (nπ*) excitation studied by transient absorption spectroscopy and *ab initio* molecular dynamics†

Till Reichenauer,‡[a] Marcus Böckmann,‡[b] Katharina Ziegler,[c] Vikas Kumar,[a] Bart Jan Ravoo, *[c] Nikos L. Doltsinis *[b] and Sebastian Schlücker *[a]

Received 22nd January 2024,
Accepted 4th March 2024

DOI: 10.1039/d4cp00295d

rsc.li/pccp

Arylazopyrazoles (AAPs) are an important class of molecular photoswitches with high photostationary states (PSS) and long thermal lifetimes. The ultrafast photoisomerization of four water-soluble arylazopyrazoles, all of them featuring an *ortho*-dimethylated pyrazole ring, is studied by narrowband femtosecond transient absorption spectroscopy and *ab initio* molecular dynamics simulations. Upon S_1 (nπ*) photoexcitation of the planar *E*-isomers (*E*-AAPs), excited-state bi-exponential decays with time constants τ_1 in the 220–440 fs range and τ_2 in the 1.4–1.8 ps range are observed, comparable to those reported for azobenzene (AB). This is indicative of the same photoisomerization mechanism as has been reported for ABs. In contrast to the planar *E*-AAPs, a twisted *E*-AAP with two methyl groups in *ortho*-position of the phenyl ring displays faster initial photoswitching with τ_1 = 170 ± 10 fs and τ_2 = 1.6 ± 0.1 ps. Our static DFT calculations and *ab initio* molecular dynamics simulations of *E*-AAPs on the S_0 and S_1 potential energy surfaces suggest that twisted *E*-isomer azo photoswitches exhibit faster initial photoisomerization dynamics out of the Franck–Condon region due to a weaker π-coordination of the central CNNC unit to the aromatic ligands.

Open Access Article. Published on 12 March 2024. Downloaded on 3/13/2025 2:26:13 AM.
This article is licensed under a Creative Commons Attribution 3.0 Unported Licence.

Introduction

Light-driven molecular switches are promising candidates for applications such as optical data storage and photopharmacology.[1,2] An archetypical representative of photochromic molecular switches is azobenzene (AB) due to its outstanding photophysical properties, enabling an efficient $E \rightarrow Z$ and $Z \rightarrow E$ photoisomerization.[3] Rau and co-workers already demonstrated for sterically hindered ABs in the late 1980s that the $E \rightarrow Z$ and $Z \rightarrow E$ photoisomerization quantum yields approach each other when the size of the substituents is increased.[4] These early results, albeit not involving time-resolved experiments, can be indicative of faster photoisomerization of twisted *E*-isomers.

In 2014 Fuchter and co-workers presented arylazopyrazoles (AAPs) as a new class of photoswitchable azo-compounds that overcome certain limitations of AB derivatives, particularly limited $Z \rightarrow E$ backswitching performance and *Z*-isomer thermal stability.[5–7] In AAPs the steric hindrance between the two aromatic rings is reduced due to its less bulky five-membered pyrazole ring instead of a second phenyl ring in ABs. An optimized orthogonal *Z*-conformation can be achieved by adding two methyl groups at the *ortho*-positions of the pyrazole. These dimethylpyrazole-AAPs therefore have improved backswitching performance compared to their AB counterparts, showing photoconversion yields as high as >98% in the photostationary state (PSS).[5–7] Due to the growing use of AAPs as photoswitches, the question arises if the ultrafast dynamics of AAPs resemble that of AB. To the best of our knowledge, we report the first study on the ultrafast photoswitching dynamics of AAPs. Potential differences between AAPs and ABs could hypothetically arise from the dimethyl groups close to the central azo moiety. A theoretical study by Wang *et al.* concludes that these AAPs should retain the lifetimes, excitation energies, conical intersections, and barrierless S_1 potential energy surface of ABs.[8] On the other hand, this similarity suggests that AAPs inherit an imperfection in the dynamics of typical ABs: their *E*-isomer photoisomerization quantum yields are reduced in comparison to those of the *Z*-isomer due to slower $E \rightarrow Z$

[a] *Physical Chemistry I and Center for Nanointegration Duisburg-Essen (CENIDE), Universität Duisburg-Essen, 45141 Essen, Germany*
[b] *Institute of Solid-State Theory and Center for Multiscale Theory and Computation, Universität Münster, 48149 Münster, Germany. E-mail: nikos.doltsinis@uni-muenster.de*
[c] *Organic Chemistry Institute and Center for Soft Nanoscience (SoN), Universität Münster, 48148 Münster, Germany. E-mail: b.j.ravoo@uni-muenster.de*

† Electronic supplementary information (ESI) available. See DOI: https://doi.org/10.1039/d4cp00295d

‡ These authors contributed equally.

This journal is © the Owner Societies 2024

Open Access Article. Published on 12 March 2024. Downloaded on 3/13/2025 2:26:13 AM.
This article is licensed under a Creative Commons Attribution 3.0 Unported Licence.

than $Z \rightarrow E$ switching dynamics.[9,10] The groups of Herges and Temps found a solution for this problem: dihydrodibenzodiazocine, a bridged azobenzene with significantly improved $E \rightarrow Z$ quantum yields (50% instead of 24% for AB) due to the twisted preorientation of the *E*-isomer.[11] The sensitivity of lifetimes in the photo-excited state to preorientation was hypothesized to originate from an initial stabilizing force that acts against the twisting force of the azo antibonding state.[12–15]

For an *E*-AAP with two methyl groups in *ortho*-position of the phenyl ring, the DFT calculations by Böckmann and Doltsinis revealed a twisted ground-state geometry; note that in this case, the molecular twist is caused by steric hindrance in contrast to the bridged AB which, in addition to the connecting azo moiety, requires an additional covalent C–C linkage between the two rings. The experimentally demonstrated superior photoswitching dynamics of the bridged AB dihydrodibenzodiazocine with its twisted *E*-isomer in combination with the theoretically predicted twisted ground-state geometry of the *ortho*-dimethylated AAP led us to the hypothesis that the latter should also exhibit a faster photoswitching dynamics than planar *E*-AAP derivatives.[7] Therefore, we experimentally tested this hypothesis by using ultrafast transient absorption spectroscopy on four AAPs shown in Fig. 1.

The first AAP pair, comprising AAP-1 with a hydrogen atom and AAP-2 with an electron-donating methoxy group in the *para* position of the phenyl ring, has a planar *E*-isomer. The second AAP pair comprising AAP-3 with a single and AAP-4 with two methyl groups in *ortho* position of the phenyl ring has a twisted *E*-isomer. AAP-2 is a nearly binary photoswitch (>98% PSS), *i.e.*, the isolated $E \rightarrow Z$ and $Z \rightarrow E$ ultrafast photoswitching dynamics can be easily determined. Additionally, AAP-2 also has the highest $E \rightarrow Z$ photoisomerization quantum yield ($\phi_{E\rightarrow Z}$). (Fig. S1 in ref. 7). The higher steric hindrance in *E*-AAP-4 than *E*-AAP-3 results in a substantially twisted geometry.

Experiment section

Materials

All chemicals used in this study were purchased from Alfa Aesar (Karlsruhe, Germany), Sigma-Aldrich Chemie (Taufkirchen, Germany) and TCI Europe (Zwijndrecht, Belgium), and used without further purification. Solvents were dried according to conventional methods before use.

All synthesis procedures described in the following were done according to a previous publication of the Ravoo group.[7] Moisture-sensitive reactions were carried out in oven-dried glassware under an inert atmosphere. Analytical thin-layer chromatography was performed on Merck silica gel 60 F_{254} plates. Visualization of the compounds was achieved either under UV-light of 254 nm with a Dual Wavelength UV Lamp (254 nm and 366 nm) (CAMAG, Muttenz, Switzerland) or by staining with basic permanganate solution. Silica gel 60 (230–400 mesh) was used for column chromatography. NMR spectra were recorded on a Bruker AV300 (300 MHz), Bruker AV400 (400 MHz), Agilent DD2 (500 MHz) or Agilent DD2 (600 MHz) spectrometer. Chemical shifts were referenced to internal standards.

All AAPs were previously characterized in regards to their photochemical properties, photoisomerization quantum yields, photostationary states (PSS) and half-life times of the *Z* isomer.[7] For each arylazopyrazole a 5 mM aqueous solution with MilliQ water was prepared.

Methods

UV/Vis absorption spectroscopic measurements were conducted using a JASCO V650 double-beam spectrophotometer (JASCO Labor- und Datentechnik GmbH, GrossUmstadt) at 25 °C, using 1 mL low-volume disposable PMMA cuvettes (Brand GmbH & CO KG, Wertheim). The spectrometer was controlled by Spectra Manager version 2.08.04 (Jasco Labor- und Datentechnik GmbH, Gross-Umstadt). The samples were

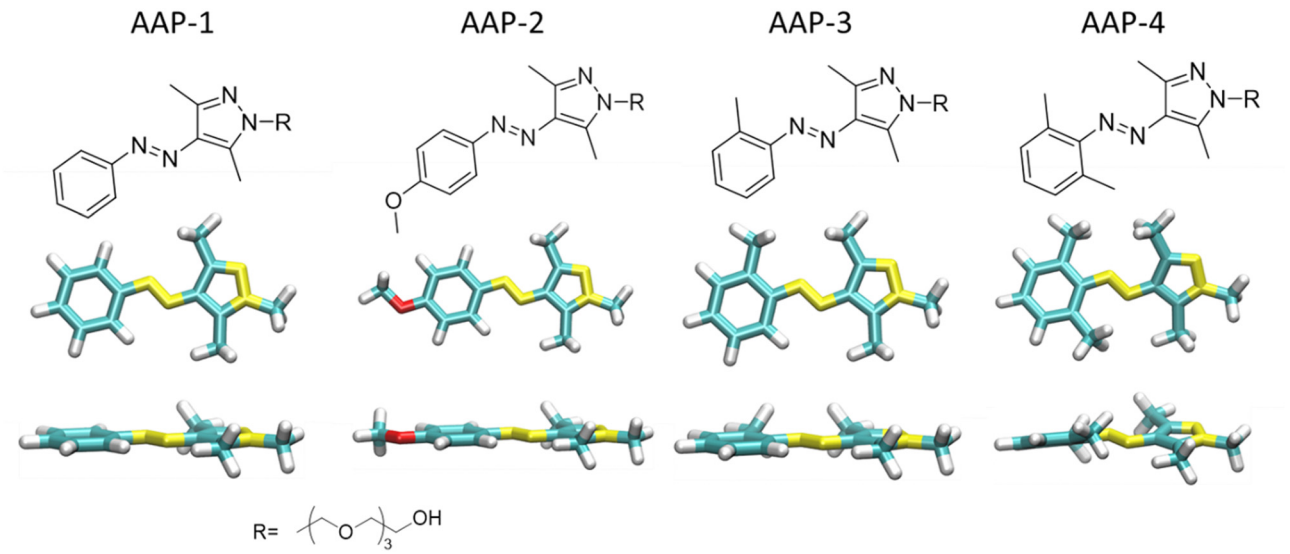

Fig. 1 Molecular structures of water-soluble *E*-AAPs 1, 2, 3 and 4 together with their optimized global minimum geometries shown in top and side view. The tetraethyleneglycol (TEG) chain is represented as a methyl group in all calculations; *cf.* ESI† for additional conformations.

Open Access Article. Published on 12 March 2024. Downloaded on 3/13/2025 2:26:13 AM.
This article is licensed under a Creative Commons Attribution 3.0 Unported Licence.

dissolved in an appropriate solvent and measured against the same solvent. More detailed information as concentrations and sample preparation, is stated in Section 1 of the ESI.†

Two different light sources were utilized for the photoswitching experiments: a 365 nm UV LED for $E \rightarrow Z$ isomerization and a green LED emitting at 530 nm for $Z \rightarrow E$ isomerization. Irradiation times are stated in the corresponding measurements section. For the ultrafast transient absorption experiments, the sample solution is additionally cycled *via* a flow system through a 2 mm thick flow-cuvette. To enrich the sample with either *E* or *Z*-isomers to its respective photostationary state, a set of the UV LEDs (total power 3 W) or the green LEDs (total power 3 W) irradiates the reservoir (*ca.* 200 ml) of the flow system for one hour before as well as during the measurement. After each measurement, the sample was replaced to mitigate the potential impact of photodegradation.

Pump and probe pulses for transient absorption measurements are generated by two wavelength tunable hybrid NOPAs (light conversion: Orpheus-F), both seeded by a 1030 nm Yb:KGW laser (light conversion: PHAROS). The first NOPA is set to 650 nm (FWHM *ca.* 20 nm). Subsequently, a prism compressor reduces the pulse duration to ~60 fs. The output of the second NOPA at 860 nm was frequency-doubled to 430 nm (FWHM *ca.* 10 nm, pulse duration ~70 fs) to be utilized as pump pulses. Pump (~1 mW) and probe (~300 μW) pulses were temporally and spatially synchronized in collinear geometry and focused on the flow cuvette using a lens (f = 100 mm). The circulation at the sample combined with 2 kHz repetition rate of pulses ensures that a fresh sample volume is probed for each pulse interaction. The pump wavelength is removed using a long-pass filter. The probe beam was collimated after the sample and measured using a silicon photodiode. The transient signal was measured using the modulation transfer technique. For this, the pump beam before the sample was chopped at 250 Hz and photodiode signal after a trans-impedance amplification is fed into a lock-in amplifier (Zürich Instruments UHFLI 600 MHz).

Transient absorption data is analyzed using the ''lsqcurvefit'' function of the Optimization Toolbox in MATLAB. For *E*-isomers, the fitting was performed over the delay time range of −0.7 to 10 ps using the sum of two Gaussian convoluted exponentials. In the case of *Z*-isomers, fitting was done in the range of −0.7 to 5 ps using a mono-exponential Gaussian convoluted function. Moreover, for both isomers, a rising exponential step function was included to take into account photoproduct formation. The plots were finally produced using OriginPro (OriginLab Corp., Northampton, Massachusetts, USA).

Results and discussion

Experimental section

Fig. 2 shows the ground state UV/Vis absorption spectra of AAP-1 as a representative AAP compound (for UV/Vis absorption spectra of other compounds see Fig. S1, for theoretical spectra Fig. S8, ESI†). Displayed are the spectra of unirradiated AAP-1 (black) together with those obtained after exhaustive irradiation with

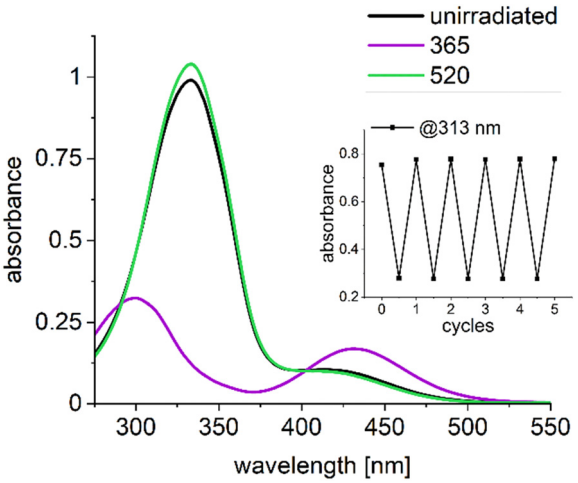

Fig. 2 UV/Vis absorption spectra of unirradiated AAP-1 (black) in water together with those obtained after irradiation with 365 nm light (*Z*-enriched PSS) and irradiation with 520 nm light (*E*-enriched PSS) at 50 μM concentration and 12.5 mm absorption pathlength. The inset shows that AAP-1 is stable under reversible photoswitching.

365 nm light (*Z*-enriched PSS, magenta) and irradiation with 520 nm light (*E*-enriched PSS, green). The absorption spectrum of the *Z*-enriched PSS (magenta) has two maxima at 312 nm and 440 nm, which are assigned to ππ* and nπ* transitions, respectively. For the *E*-enriched PSS (green), the maximum for the ππ* transition is shifted from 311 nm to 347 nm due to the extended π-conjugation in the planar *E*-isomer; the corresponding absorbance at the maximum is increased by a factor of *ca.* 2.8 due to the increased oscillator strength. The contribution of the nπ* transition at 400 nm is visible as a shoulder. A more detailed discussion of the UV/Vis absorption spectra of AAPs is available in the first report by Fuchter and co-workers.[5] The inset in Fig. 2 shows that AAP-1 is stable under reversible photoswitching as was expected.[7]

For experimentally testing our hypothesis that twisted *E*-isomers exhibit faster photoisomerization dynamics than planar *E*-isomers, we conducted femtosecond transient absorption (fs-TA) studies on all four AAPs from Fig. 1. This requires selectively populating the S_1 (nπ*) state and selectively probing it. The transition to the lowest excited state, the S_1 (nπ*), as opposed to the S_2 (ππ*) state, was chosen due to the reduced complexity in kinetics and since for AB as the ''gold standard'' it was found that for both excitations, the main isomerization movement occurs on the nπ* energy surface.[16] Since all four AAP derivatives have corresponding absorption maxima for this electronic transition in the range 400–440 nm, we chose 430 nm as the pump wavelength. The nπ* excitation may seem to emphasize the *Z*-dynamics due to its greater absorption in the ground state, for ABs this impact is however compensated due to a larger *E*-isomer nπ* excited state absorption oscillator strength that leads to a transient absorption signal of a similar order of magnitude.[17]

The choice of the probe wavelength requires knowledge of the electronic absorption of AAPs in the S_1 (nπ*) state. In the case of AB, this state is broadly accessible from 500–690 nm

 This journal is © the Owner Societies 2024

Open Access Article. Published on 12 March 2024. Downloaded on 3/13/2025 2:26:13 AM.
This article is licensed under a Creative Commons Attribution 3.0 Unported Licence.

with a resonance centered at 530 nm for *E*-AB and 540 nm for the *Z*-AB.[17] The transient absorption spectrum of AAP-2, *i.e.*, the AAP with the highest PSS (>95%) and therefore the "purest *E*-enriched compound" of all four AAPs, exhibits a broad electronic resonance centered at 575 nm (Fig. S6, ESI†). The observed red shift in the ESA spectrum of *E*-AAP-2 compared to AB was expected since the absorption spectra of AAPs in the electronic ground state S_0 are generally red-shifted compared to those of ABs.[5] In order to ensure that the S_1 ($n\pi^*$) state is selectively probed, the probe wavelength must be resonant with the ESA and should be off-resonant with the S_0 ground state. We therefore chose 650 nm as the probe wavelength as a good compromise for matching these criteria. Thus, the probe wavelength is red-shifted to the maximum ESA for selectively observing the ultrafast lifetimes associated with the molecule's movement on the S_1 ($n\pi^*$) potential energy surface, minimizing interfering transient contributions such as photoproduct absorption (PA), ground state bleach (GSB) and hot ground state absorption (HGSA).[17,18]

The ESA signal observed could be attributed to the $S_1 \rightarrow S_5$ excitation by inspection of the oscillator strengths of TDDFT transition dipole moments (see Fig. S9, ESI†).

Based on fs-TA studies on AB, we expected two dominant time constants that describe the ultrafast photoisomerization of the *E*-isomers of all four AAPs: one very fast component with $\tau_1 < 1$ ps (AB $\approx$ 300 fs) and a slower component with $\tau_2 > 1$ ps (AB: $\approx$2–3 ps).[19–21] There is a wide consensus that the dominant short lifetime τ_1 corresponds to the initial rapid directed movement out of the Franck–Condon region towards a conical intersection.[18,19,21–23] In contrast, the assignment of the second decay component in ABs remains debated. Many studies assign the slower time constant τ_2 to the movement from the conical intersection in the excited state back to the ground state.[20–23] On the other hand, other studies attribute τ_2 to the relaxation to a dark *E*-intermediate on the S_1 ($n\pi^*$) potential energy surface.[17,24–26] In both interpretations, τ_2 reflects a lower boundary for the completed photoisomerization. In contrast to the *E*-isomer, the dynamics of the *Z*-isomer exhibit a mono-exponential decay.[19]

Since all selected AAPs, apart from AAP-2, do not possess isomerically pure photostationary states, the transients contain contributions from both isomers. In the absence of additional species, the signal can therefore be described as a linear combination of the signals from the *E*- and *Z*-isomers. Their relative contributions, *i.e.*, the coefficient for the linear combination, require the determination of the photostationary state (PSS), *i.e.*, the information about the position of the photochemical equilibrium. The PSS values for all four AAPs were already reported in ref. 7. For the purpose of this study, the PSS values were accurately remeasured by ^{1}H NMR spectroscopy. In short, a solution (c = 200 μM) of each AAP in D_2O was irradiated with UV light (to obtain the $E \rightarrow Z$ PSS) or with green light (to obtain the $Z \rightarrow E$ PSS). The fraction of each isomer in each sample was determined by integration of the peaks for the methyl groups at AAP, which have a distinct chemical shift. The resulting values for AAP 1-4 are listed in Table 1. ^{1}H NMR spectra and further experimental details are reported in Section 3 of the ESI† (see Fig. S2–S5). Significantly, the AAP-2 sample we examined, which was previously documented to exhibit a PSS exceeding 98% in both isomeric directions, displayed a PSS of only 96% for the *E*-isomer and 95% for the *Z*-isomer. Such variations may potentially stem from minute differences in conditions such as concentration, light source, sample irradiation time, and intensity.

Table 1 PSS values after irradiation with 530 nm ($Z \rightarrow E$) and 365 nm ($E \rightarrow Z$) light determined by ^{1}H NMR (for procedure and spectra, refer to Fig. S2–S5, ESI)

	$PSS_{E\rightarrow Z}$ (%)	$PSS_{Z\rightarrow E}$ (%)
AAP-1	92	89
AAP-2	96	95
AAP-3	93	80
AAP-4	72	67

With these experimentally determined PSS values and the measured transient absorbances $A(t)$ of *E*- and *Z*-enriched samples, the "pure" transient signals of *E*- and *Z*-isomers, respectively, were extracted. This is done by solving the equation system derived from the linear combination of signals for each isomer. The resulting expression is as follows:

$$A_{E,Z}(t) = \frac{A_{E,Z,\mathrm{Rich}}(t)\mathrm{PSS}_{Z,E} + \left(\mathrm{PSS}_{E,Z} - 1\right)A_{Z,E,\mathrm{Rich}}(t)}{\mathrm{PSS}_{E,Z} + \mathrm{PSS}_{Z,E} - 1}$$

The left side of Fig. 3 presents the absorption transients for all four *Z*-isomers in a single graph for a direct visual comparison. For this the transients are normalized in the time-delay window between 0 ps and 1.5 ps. Overall, the observed *Z*-AAP time constant values are all relatively close to those observed for *Z*-ABs (*ca.* 100 fs).[17,19–21]

In contrast to the *Z*-isomers, the *E*-isomers exhibit a significantly slower initial dynamic and a non-negligible contribution

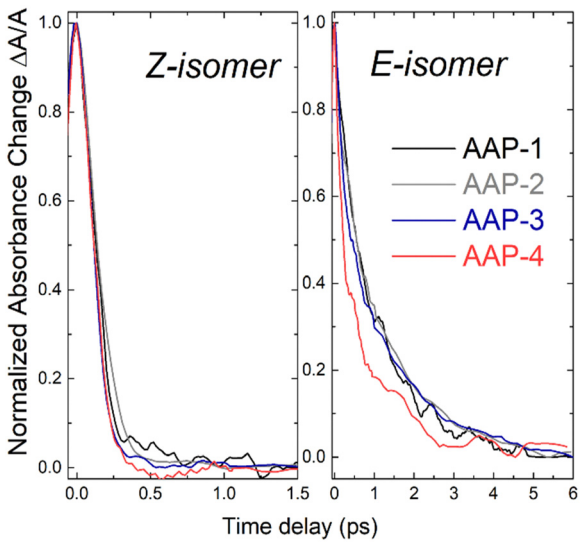

Fig. 3 Normalized transient absorption (λ_{pump} = 430 nm, λ_{probe} = 650 nm, c = 5 mM) of the four AAPs in water for the *Z*-isomer (left) and *E*-isomer (right).

Open Access Article. Published on 12 March 2024. Downloaded on 3/13/2025 2:26:13 AM.
This article is licensed under a Creative Commons Attribution 3.0 Unported Licence.

on the >1 ps time scale. Data for the *E*-isomer is therefore fitted with an additional exponential decay term. The resulting fits are displayed in Fig. 4. The more significant step in transient absorption (gray curves in Fig. 4) for *E*-AAPs in comparison to *Z*-AAPs is likely to originate from product absorption since *Z*-AAPs have a larger ground state absorption than *E*-isomers at the probe wavelength. The rise of this absorption step, represented by a rise time constant, corresponds well to the slower decaying component. Therefore, we believe that AAPs also behave analogous to ABs in the interpretation that τ_2 represents the time for completed isomerization and the absorption step correlates to the ground state absorption of the newly generated *Z*-isomers. For this reason, the second slow time constant and the time constant of the rising exponential term were fixed to be equal. The accuracy of the fits ($R^2 > 0.99$) indicates that the ultrafast dynamics of all dimethyl-AAPs resemble that of AB, for which a similar biphasic decay after nπ*-excitation was reported.[19,21] Again, as for the *Z*-isomers, the right section of Fig. 3 presents the transients for all four *E*-isomers in a single graph for direct visual comparison.

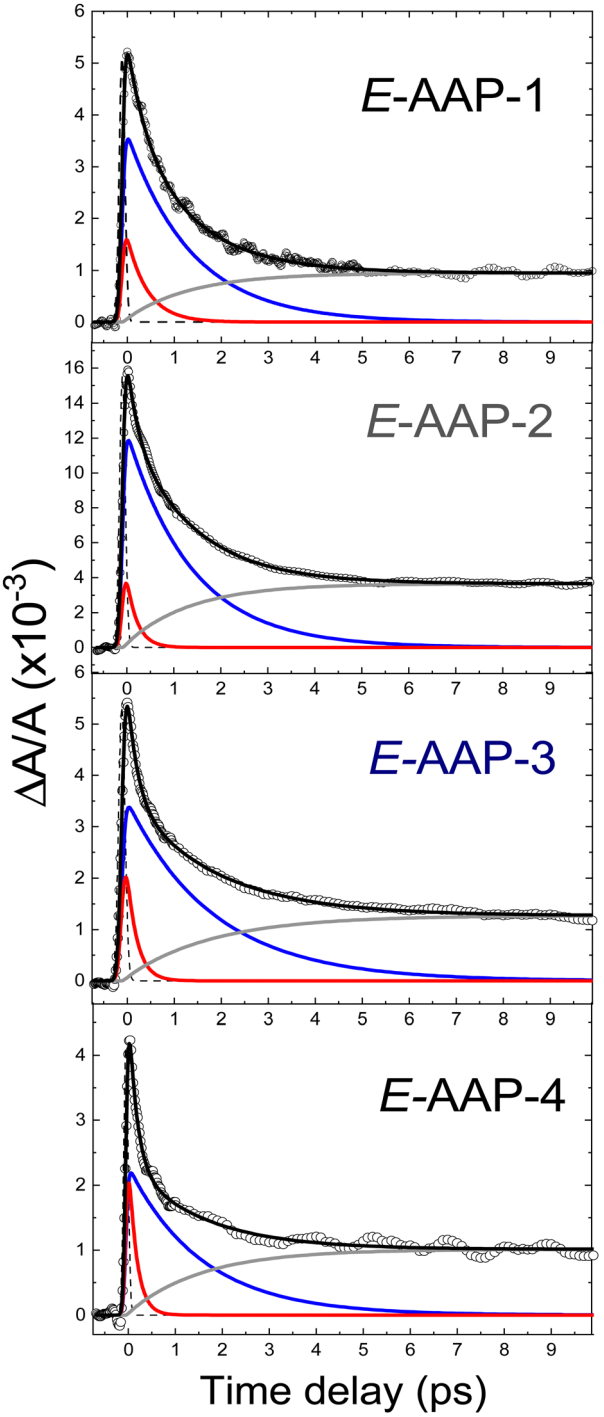

Fig. 4 Data analysis of the transient absorption data for the *E*-isomer (shown as circles). The overall fit function is depicted in black, encompassing components of exponential decay (red, blue) and permanent absorption (gray). Furthermore, displayed is the IRF represented by a Gaussian function (dashed line).

Table 2 lists the extracted τ_1 lifetimes for *E*-AAP-1 (440 fs), *E*-AAP-2 (220 fs) and *E*-AAP-3 (210 fs), all in good agreement with those measured for *E*-AB in ethanol (320 fs) and DMSO (340 fs)[19–21] as well as with the azoheteroarene photoswitch thiophenylazobenzene (400 fs).[27] For *E*-AAP-4, on the other hand, a significant reduction in τ_1 (170 fs) is observed. This observation supports the hypothesis that twisted *E*-AAPs exhibit faster initial photoisomerization dynamics. Further support comes from *ab initio* molecular dynamics calculations (*vide infra*). The relative amplitudes (A_2/A_1) of the slower (τ_2) and faster (τ_1) decay components are reported in Table 2. The results show that *E*-AAP-2 possesses a substantially larger slow decay portion in comparison to *E*-AAP-1 and *E*-AAP-4.

The τ_2 lifetimes of all four *E*-AAPs are between 1.4 ps and 1.8 ps. These τ_2 lifetimes are smaller (<2 ps) than those for typical ABs (2–3 ps), but distinctly longer than that (0.27 ps) for the bridged AB (dihydrodibenzodiazocine). In contrast to the faster initial dynamics described by τ_1 that differs by a factor of about 3 between planar *E*-AAP-1 (440 fs) and twisted *E*-AAP-4 (160 fs), the slower dynamics described by τ_2 is similar for both planar and twisted *E*-AAPs; for example, *E*-AAP-1 (1.4 ps) and *E*-AAP-4 (1.6 ps) show only marginal differences on that timescale. This suggests that – despite their differences in the faster initial movement away from the Franck–Condon region (τ_1) – all *E*-isomers encounter a similar bottleneck for photoisomerization on the S_1 potential energy surface and/or the conical intersection (τ_2).

Theoretical section

We begin our theoretical analysis by examining the minimum energy potential (MEP) scans presented in Fig. 6 for the rotation of the phenyl (top panel) and pyrazole ring (bottom panel) of the AAPs under investigation. All scans were performed with a step size of 5° starting from the corresponding minima presented in Fig. 1 (see Table S1 for relative energies of structural conformers, ESI†). It is clearly seen that the MEP for the rotation of the 5-membered pyrazole ring is rather stiff and similar for all species, with the global minimum at 0° (s-*anti* conformation, *cf.* Fig. 1), a barrier of 0.3–0.5 eV at roughly 90°, and a slightly elevated (by <0.05 eV) local minimum at 180°

 This journal is © the Owner Societies 2024

Open Access Article. Published on 12 March 2024. Downloaded on 3/13/2025 2:26:13 AM.
This article is licensed under a Creative Commons Attribution 3.0 Unported Licence.

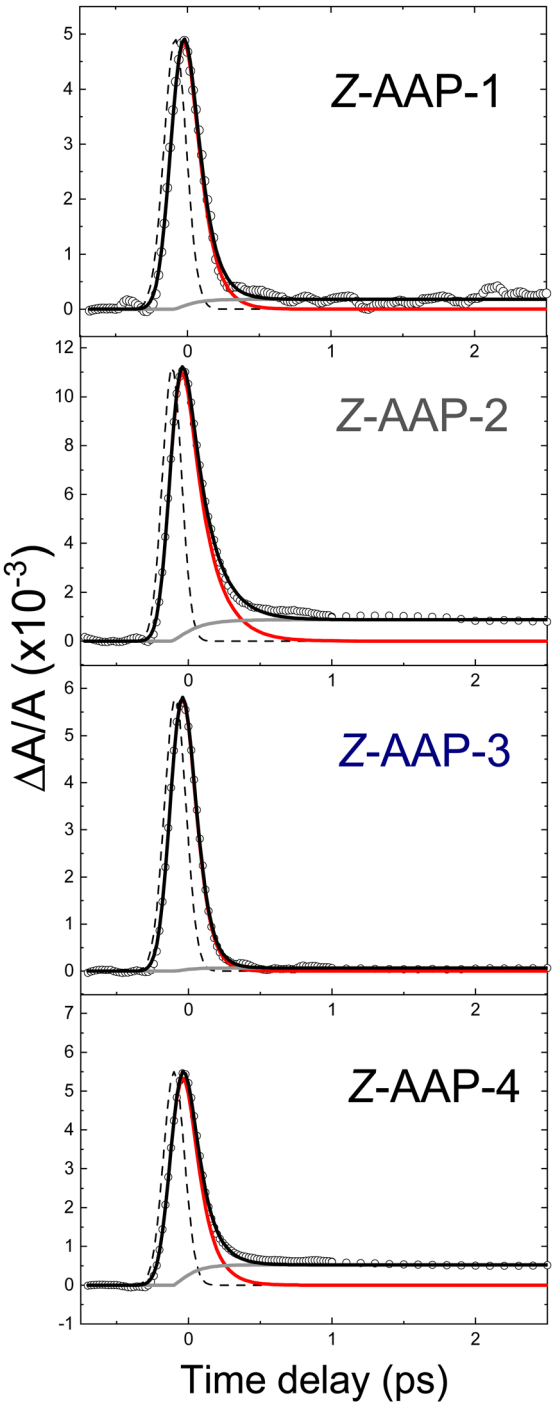

Fig. 5 Data analysis of the transient absorption data for the *Z*-isomer.

(s-*syn* conformation). We note in passing that for AAP-2 the minimum is slightly shallower, allowing for a mildly more pronounced ring wagging motion (*vide infra*). In contrast, the curves for the rotation of the 6-membered phenyl ring show striking differences (top panel). Compared to all other species, AAP-4 has a very low rotational barrier of 0.09 eV at 90° and the global minimum is shifted to *ca.* 30° (or 150° by symmetry). The potentials for the unsubstituted (AAP-1) and para-substituted (AAP-2) structures resemble those for the 5-membered ring

Table 2 Time constants τ_1 and τ_2 in ps determined from bi-exponential (*E*) and monoexponential fits (*Z*) along with standard errors obtained from the fitting procedure and with consideration to the IRF in the experiment (see Fig. 4 (*E*) and Fig. 5 (*Z*) for the fits)

	E-Isomer			*Z*-Isomer
	τ_1 (ps)	τ_2 (ps)	A_2/A_1	τ_1 (ps)
AAP-1	0.44 ± 0.02	1.4 ± 0.1	5.9 ± 0.9	0.1 ± 0.01
AAP-2	0.22 ± 0.01	1.4 ± 0.05	13.8 ± 0.2	0.15 ± 0.01
AAP-3	0.21 ± 0.01	1.8 ± 0.05	9.2 ± 0.2	<0.07 (IRF limited)
AAP-4	0.17 ± 0.01	1.6 ± 0.1	6.6 ± 0.3	<0.07 (IRF limited)

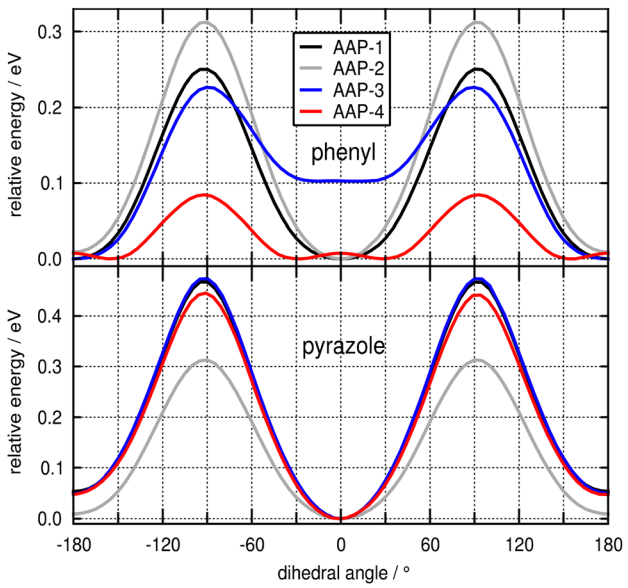

Fig. 6 Minimum energy potential scans in the ground state for the dihedral angle coordinate describing the rotation of the phenyl ring (top) and pyrazole ring (bottom) attached to the azo moiety of the different AAPs.

(*i.e.* minimum at 0°, maximum at about 90°), whereas the curve for the mono-*ortho* substituted AAP-3 requires closer inspection. Due to the asymmetry in the two *ortho* positions, there are two different minima: the global minimum at 180° (*cf.* Fig. 1) similar in stiffness to AAP-1, and a local minimum at about 5°, 0.10 eV higher in energy (see also Table S1, ESI†), similar in width to AAP-4. The latter can be attributed to the unfavourable interaction of the methyl group with the distal nitrogen atom lone pair ('steric hindrance'). As this interaction is present in both minima of the symmetric di-*ortho* AAP-4, it explains the low energy barrier between them.

The above conclusions on the ring flexibility of the four AAPs derived from static calculations are corroborated by *ab initio* MD simulations at 300 K in the ground state (see Fig. S18 and S19, ESI†). The data reveals a torsional phenyl ring fluctuation of about ±30° for the planar AAP-1 and AAP-2, similar to the parent compound AB.[28] The mono-*ortho* substituted AAP-3 is even seen to overcome the barrier at 90° within the simulated duration of *ca.* 20 ps. AAP-4 shows – in accordance with the low energy barrier – an extremely broad distribution of rotation

Open Access Article. Published on 12 March 2024. Downloaded on 3/13/2025 2:26:13 AM.
This article is licensed under a Creative Commons Attribution 3.0 Unported Licence.

angles around a maximum at 43° with a half-width of 41° (*cf.* Fig. S19, ESI†). This different behavior of the *ortho*-substituted AAP-3 and AAP-4 in contrast to AAP-1 and AAP-2 in the ground state can be understood in terms of the molecular frontier orbitals presented in Fig. S20 (ESI†). It is seen that the *ortho*-methyl groups constructively contribute to the conjugation of the π-system extending from the phenyl ring across the azo nitrogen double bond to the pyrazole ring. Importantly this explains (i) the rather stiff MEP curves for the ring rotation of AAP-1 and AAP-2 (because the π-system conjugation breaks down upon deviation from planarity), and (ii) the significantly reduced barrier for the phenyl ring rotation in AAP-4, because conjugation can still be mediated *via* the two *ortho*-methyl groups. This is further supported by an analysis of the overall π-system in terms of Wiberg bond indices (see ESI,† Section S5.7).

In summary, the analysis of the ground state properties clearly reveals that AAP-4 is distinguished from the other species by allowing for an – on average – much larger out-of-plane rotation of the phenyl ring.

In order to theoretically probe the escape from the Franck–Condon region after vertical excitation to the S_1 state, we have – as a first step – investigated the vibrational normal modes obtained for the ground state structures in the vertically excited S_1 state. Here, the first mode with imaginary frequency (depicted in Fig. S10 for E-AAP-1 and E-AB, ESI†) reveals the 'downhill' direction. Note, that for AB the ground state optimized E structure corresponds to a transition state in the S_1 state (*i.e.*, there is only one imaginary frequency and the energy gradient vanishes), which may lead to a spurious S_1 minimum at a CNNC dihedral angle of 180° when symmetry is employed in electronic structure calculations.

As is readily seen, the motion is dominated by a concerted out-of-plane twist of the two nitrogen atoms of the azo group double bond, which changes the CNNC dihedral from 180° towards 90° (see Fig. S11 for an analysis of the characteristic motion along this mode, ESI†), thereby allowing for a decoupling of the two p-orbitals involved in the *anti*-bonding π* molecular orbital (see Fig. S12 for a visualisation of the frontier orbitals, ESI†). This motion is equivalent to the pedal-like 'hula-twist' mechanism reported for S_1 photoisomerization of AB[17,29–31] and it is in line with elementary electronic structure considerations for π* excitations of a N=N double bond.[32,33]

In this context, we would like to emphasize that the inversion photoisomerization pathway, which is often discussed in the literature, cannot account for any relaxation of the *anti*-bonding character of the π* molecular orbital populated upon excitation, since the two p-orbitals remain antiparallel. Thus, from the viewpoint of electronic structure theory, the inversion pathway is implausible.

The competing driving forces, *i.e.* the decoupling of the antibonding nitrogen p-orbitals and the coupling of each nitrogen p-orbital to the π-system of its adjacent ring structure can be conveniently visualized by plotting the plane normal vectors of the two rings and the coordination planes of the two central nitrogen atoms as shown in Fig. S13 (ESI†). The fact that, for the *Z* isomer, the two ring system are out of conjugation with the azo group readily accounts for $Z \rightarrow E$ photoisomerisation generally being much faster than in the $E \rightarrow Z$ direction. This effect also accounts for the fast $E \rightarrow Z$ photoisomerization of bridged AB.[12]

To further corroborate this point, we probed the escape from the Franck–Condon region by means of steepest descent geometry optimization in the S_1 state following an approach by Slavov *et al.*[27] Due to the flatness of the potential energy surface in this region, no change in the CNNC dihedral angle was observed after more than 150 steps when starting from the optimized ground state structure (Fig. S14, ESI†). However, when the initial structure is prepared with the phenyl ring twisted by as little as 10°, the CNNC dihedral decreases rapidly to 120° in about 60 steps. For AAP-4 this decrease is achieved in about 30 steps starting from the minimum structure as it has (*vide supra*) the phenyl ring twisted by 27° (see Fig. S15, ESI†).

Although the steepest descent path sheds some light on the role of the phenyl ring twist, it cannot provide any information on the dynamical photoisomerization mechanism. Therefore, we performed *ab initio* MD runs starting from the corresponding S_0 minima with zero initial velocities (this way, we obtain an unbiased 'fingerprint' of the curvature of the excited state potential energy surface in this pivotal region responsible for the relaxation time τ_1). The resulting time evolutions obtained for the four AAPs under investigation are presented in Fig. 7 for the *E* conformers (top panel), and the Z conformers (bottom panel).

Here, the CNNC dihedral angle indicating the progress of the photoisomerization – which proceeds by the pedal-like hula-twist mechanism – is plotted down to 90° (up to 90° for the *Z* conformers), *i.e.* near the S_1 minimum and conical intersection. While all four *Z*-AAPs (and the parent compound AB, included here as a reference) show (the expected) ultrafast decay from the Franck–Condon region, for the *E*-AAPs ultrafast decay is only observed for *E*-AAP-4, whereas all other species initially remain stuck at around 180° for a significant amount of time before twist motion sets in, which we attribute to their preferred (near-)planar phenyl ring orientation in the ground state (similar results were obtained for photoisomerization dynamics in the T_1 state, see Fig. S23, ESI†). Thus, we conclude that the experimentally found enhanced transient absorption decay of *E*-AAP-4 (as compared to AAP-1, 2, and 3) is related to the out-of-plane pre-orientation of the phenyl ring in the ground state, which in turn is due to the interaction of the two *ortho*-methyl groups with the underlying π-system.

To add further weight to this argument, we have carried out excited state simulations of *E*-AAP-1 and *E*-AAP-4 with different, specifically modified, initial torsional angles of the phenyl ring. The upper panel of Fig. 8 shows that rotating the phenyl ring by as little as 5° significantly speeds up photoisomerization. An increase to 10° further accelerates the process, reaching a timescale comparable to AAP-4. However, even larger initial twist angles, 20° or 50°, have no noticeable additional effect. Conversely, decreasing the torsional angle of AAP-4 by 20° or 25° is seen to increasingly slow down photoisomerization, while

 This journal is © the Owner Societies 2024

Open Access Article. Published on 12 March 2024. Downloaded on 3/13/2025 2:26:13 AM.
This article is licensed under a Creative Commons Attribution 3.0 Unported Licence.

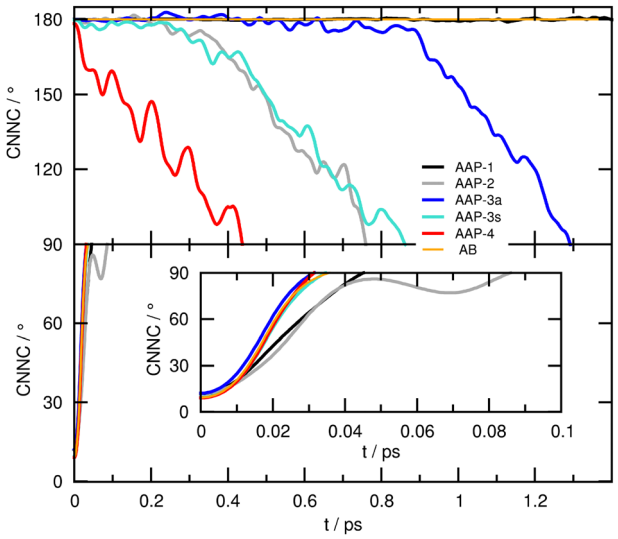

Fig. 7 *Ab initio* MD in the S_1 state: time evolution of the CNNC dihedral angle coordinate indicating the progress of the photoisomerization for the different AAPs. All trajectories are started from the corresponding S_0 minima with zero initial velocities (see text). Top panel: $E \rightarrow Z$, bottom panel: $Z \rightarrow E$. Data for the parent compound AB is shown as a reference. AAP-3a and AAP-3s refer to the *anti* and *syn* configurations of AAP-3, respectively.

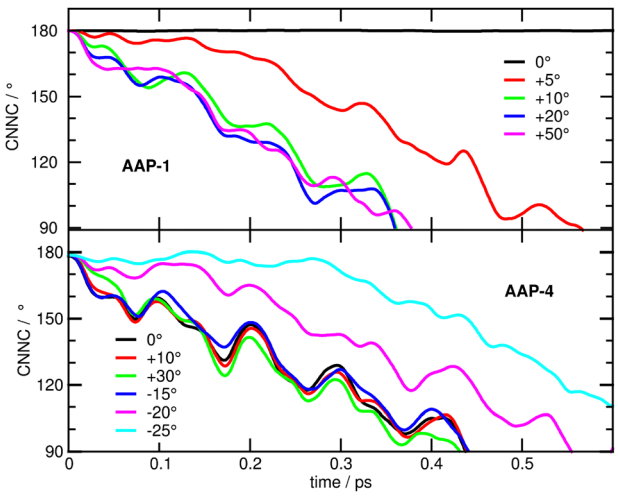

Fig. 8 Simulated time evolution of the CNNC dihedral angle of AAP-1 (upper panel) and AAP-4 (lower panel) for different initial torsional angles of the phenyl ring relative to the optimized ground state value.

increasing the torsional angle by up to 30° does not speed up the dynamics (Fig. 8, lower panel).

Conclusions

This initial study on the ultrafast photoswitching dynamics of AAPs suggests that their planar representatives, namely AAP-1 and AAP-2, closely resemble the dynamics observed for conventional ABs that can be described by a bi-exponential decay with fast (τ_1) and slower (τ_2) components. Our hypothesis that those AAP photoswitches that are sufficiently twisted in their electronic ground state (DFT calculations) exhibit an accelerated initial ultrafast dynamics (τ_1) was corroborated by narrowband femtosecond transient absorption spectroscopy *via* the reduction of τ_1 from 220–440 fs for *E*-AAP-1 (440 fs), *E*-AAP-2 (220 fs) and *E*-AAP-3 (210 fs) to 170 fs for *E*-AAP-4. Our *ab initio* molecular dynamics simulations in the excited state S_1 ($n\pi^*$) support our experimental findings for the rapid initial photodynamics (τ_1) on the S_1 surface: *E*-AAP-1 is metastable in the Franck–Condon region, while both *E*-AAP-2 and *E*-AAP-3 exhibit instability, but decay at a slower rate compared to that of *E*-AAP-4.

Our experimental observation of faster τ_1 decay for *E*-AAP-4 is also in line with earlier experimental[14] and theoretical[12] results for the rigid and twisted bridged AB dihydrodibenzodiazocine (DDD) synthesized by the Herges group. For this rigid molecular switch, the Temps group identified a rather pronounced difference between the twisted AB ($\tau_1 < 50$ fs and $\tau_2 = 270$ fs) and conventional AB ($\tau_1 \approx 300$ fs and $\tau_2 \approx 2$–3 ps).[14] Subsequent *ab initio* molecular dynamics studies demonstrated that the adjacent arene π-system orientation plays a pivotal role in the photoisomerization dynamics of the azo chromophore.[12] Overall, we attributed this discrepancy between these two pairs – twisted *vs.* planar *E*-AAPs and the twisted & bridged AB DDD – to the conformational flexibility of the AAPs in their electronic ground state at room temperature that strongly affects the initial fast photodynamics on their S_1 surface.

On the other hand, the slower picosecond dynamics (τ_2) remains unchanged in twisted *E*-AAP-4; this suggests that unlike in dihydrodibenzodiazocine, the $E \rightarrow Z$ isomerization remains impeded. The unaltered τ_2 lifetime may therefore explain why AAP-4 does not possess a dramatic improvement in quantum yields as reported for bridged azobenzene.

Future studies on the photoswitching behavior of *E*-AAPs should explore the capabilities of experimental setups with higher temporal resolution in combination with broadband transient absorption. This could improve the accuracy of the determined faster time constants τ_1 as well as potentially identify spectral shifts in the ESA spectrum.

Finally, our findings from femtosecond time-resolved optical spectroscopy in combination with *ab initio* molecular dynamics simulations may, in a prognostic approach, guide the design of improved AAP photoswitches. For example, the excellent photoswitching behavior of the planar AAP-2 in terms of nearly 100% PSS could be combined with the superior photoswitching dynamics of the twisted AAP-4 by using a combination of both methoxy substitution at the *para*-position of the phenyl ring and two methyl groups at the *ortho*-position of the same ring in addition to the two-methyl groups in *ortho*-position of the pyrazole.

Author contributions

TR: transient absorption measurements, data analysis and interpretation, manuscript writing; MB: *ab initio* molecular dynamics simulations and interpretation, conception of figures, manuscript writing; KZ: synthesis and characterization of

arylazopyrazoles, manuscript writing; VK: transient absorption measurements; BJR, ND and SeS: project idea and supervision, data interpretation, conception of figures, manuscript writing.

Conflicts of interest

There are no conflicts to declare.

Acknowledgements

This work was funded by the German Research Foundation (DFG) within the Collaborative Research Center 1242 ''Non-equilibrium Dynamics of Condensed Matter in the Time Domain'' (project A04, project ID 278162697) and the Collaborate Research Center 1459 ''Intelligent Matter'' (projects A04 and B02, project ID 433682494).

References

1 M. Sauer, *Proc. Natl. Acad. Sci. U. S. A.*, 2005, **102**, 9433.
2 L. Andruzzi, A. Altomare, F. Ciardelli, R. Solaro, S. Hvilsted and P. S. Ramanujam, *Macromolecules*, 1999, **32**, 448.
3 H. M. D. Bandara and S. C. Burdette, *Chem. Soc. Rev.*, 2012, **41**, 1809.
4 H. Rau and S. Yu-Quan, *J. Photochem. Photobiol., A*, 1988, **42**, 321.
5 C. E. Weston, R. D. Richardson, P. R. Haycock, A. J. P. White and M. J. Fuchter, *J. Am. Chem. Soc.*, 2014, **136**, 11878.
6 L. Stricker, E.-C. Fritz, M. Peterlechner, N. L. Doltsinis and B. J. Ravoo, *J. Am. Chem. Soc.*, 2016, **138**, 4547.
7 L. Stricker, M. Böckmann, T. M. Kirse, N. L. Doltsinis and B. J. Ravoo, *Chem. – Eur. J.*, 2018, **24**, 8639.
8 Y.-T. Wang, X.-Y. Liu, G. Cui, W.-H. Fang and W. Thiel, *Angew. Chem., Int. Ed.*, 2016, **128**, 14215.
9 S. Yuan, Y. Dou, W. Wu, Y. Hu and J. Zhao, *J. Phys. Chem. A*, 2008, **112**, 13326.
10 I. Conti, M. Garavelli and G. Orlandi, *J. Am. Chem. Soc.*, 2008, **130**, 5216.
11 R. Siewertsen, H. Neumann, B. Buchheim-Stehn, R. Herges, C. Näther, F. Renth and F. Temps, *J. Am. Chem. Soc.*, 2009, **131**, 15594.
12 M. Böckmann, N. L. Doltsinis and D. Marx, *Angew. Chem.*, 2010, **122**, 3454.
13 F. Renth, R. Siewertsen and F. Temps, *Int. Rev. Phys. Chem.*, 2013, **32**, 1.
14 R. Siewertsen, J. B. Schönborn, B. Hartke, F. Renth and F. Temps, *Phys. Chem. Chem. Phys.*, 2011, **13**, 1054.
15 C.-W. Chang, Y.-C. Lu, T.-T. Wang and E. W.-G. Diau, *J. Am. Chem. Soc.*, 2004, **126**, 10109.
16 H. Satzger, C. Root and M. Braun, *J. Phys. Chem. A*, 2004, **108**, 6265.
17 M. Quick, A. L. Dobryakov, M. Gerecke, C. Richter, F. Berndt, I. N. Ioffe, A. A. Granovsky, R. Mahrwald, N. P. Ernsting and S. A. Kovalenko, *J. Phys. Chem. B*, 2014, **118**, 8756.
18 J. Bahrenburg, K. Röttger, R. Siewertsen, F. Renth and F. Temps, *Photochem. Photobiol. Sci.*, 2012, **11**, 1210.
19 T. Nägele, R. Hoche, W. Zinth and J. Wachtveitl, *Chem. Phys. Lett.*, 1997, **272**, 489.
20 I. K. Lednev, T.-Q. Ye, R. E. Hester and J. N. Moore, *J. Phys. Chem.*, 1996, **100**, 13338.
21 H. Satzger, S. Spörlein, C. Root, J. Wachtveitl, W. Zinth and P. Gilch, *Chem. Phys. Lett.*, 2003, **372**, 216.
22 F. Tatsuya, A. S. Yu and T. Tahei, *Bull. Chem. Soc. Jpn.*, 2002, **75**, 1031.
23 D. P. Hoffman and R. A. Mathies, *Phys. Chem. Chem. Phys.*, 2012, **14**, 6298.
24 L. Wang, W. Xu, C. Yi and X. Wang, *J. Mol. Graphics Modell.*, 2009, **27**, 792.
25 C. J. Otolski, A. M. Raj, V. Ramamurthy and C. G. Elles, *Chem. Sci.*, 2020, **11**, 9513.
26 K. M. Krawczyk, R. L. Field, L. C. Liu, M. Dong, G. A. Woolley and R. D. Miller, *Can. J. Chem.*, 2019, **97**, 488.
27 C. Slavov, C. Yang, A. H. Heindl, H. A. Wegner, A. Dreuw and J. Wachtveitl, *Angew. Chem., Int. Ed.*, 2020, **59**, 380–387.
28 M. Böckmann, C. Peter, L. D. Site, N. L. Doltsinis, K. Kremer and D. Marx, *J. Chem. Theory Comput.*, 2007, **3**, 1789.
29 M. Böckmann, N. L. Doltsinis and D. Marx, *Phys. Rev. E*, 2008, **78**, 036101.
30 M. Böckmann, N. L. Doltsinis and D. Marx, *J. Phys. Chem. A*, 2010, **114**, 745.
31 O. Weingart, Z. Lan, A. Koslowski and W. Thiel, *J. Phys. Chem. Lett.*, 2011, **2**, 1506.
32 R. B. Woodward and R. Hoffmann, *Angew. Chem., Int. Ed. Engl.*, 1969, **8**, 781.
33 M. Klessinger and J. Michl, *Excited States and Photochemistry of Organic Molecules*, VCH Publishers, New York, 1995.

Open Access Article. Published on 12 March 2024. Downloaded on 3/13/2025 2:26:13 AM. This article is licensed under a Creative Commons Attribution 3.0 Unported Licence.

 This journal is © the Owner Societies 2024